Re-understanding the in-plane hygro-expansion of freely and restrained dried paper handsheets

RE-UNDERSTANDING THE IN-PLANE HYGRO-EXPANSION OF FREELY AND RESTRAINED DRIED PAPER HANDSHEETS

*Niels Vonk, Ron Peerlings, Marc Geers and Johan Hoefnagels**

Eindhoven University of Technology, Eindhoven, The Netherlands

ABSTRACT

The larger hygro-expansivity of freely compared to restrained dried handsheets has been intensively studied during the past decades. To investigate the role of the fibers forming the sheets on this complex phenomenon, in this work, the hygro-expansivity of fibers picked from freely and restrained dried handsheets is characterized. To do so, a versatile, highly accurate, fiber hygro-expansion methodology based on Global Digital Height Correlation is proposed, which enables identification of the transient full-field hygro-expansivity of single paper fibers. It was found that the longitudinal, transverse and shear hygro-expansivity of fibers picked from freely dried handsheets is significantly larger than fibers picked from the restrained dried handsheet. Furthermore, a restrained dried fiber can yield the hygro-expansivity of a freely dried fiber after being subjected to a sufficiently long wetting period, implying that the moisture-induced release of dried-in strain drives the hygro-expansivity differences. Finally, the sheet-scale hygro-expansivity is comparable to longitudinal fiber hygro-expansivity for both handsheet types. The presented

* Corresponding author

results are of key importance for understanding the paper hygro-mechanics and improve their applicability.

Key words: Freely dried, Full-field fiber characterization, Global Digital Height Correlation (GDHC), Hygro-expansion, Restrained dried

INTRODUCTION

Nowadays, due to environmental reasons, industrial printing companies increase the usage of water-based inks and hence the development of their ink-jet printers. Inside most ink-jet printers, the paper sheet is subjected to multiple wetting and drying (e.g., an elevated temperature) operations, while being restrained (e.g., a vacuum to maintain a flat paper sheet) or free, to attain a crisp printed sheet. However, it can occur that the paper sheet is not dried accordingly and highly unwanted phenomena, such as out-of-plane deformations (e.g., curling, cockling, and fluting) occur [1]. To optimize the printing process, the swelling characteristics of the paper sheet throughout the complete printing process needs to be characterized, in particular, the difference between freely and restrained dried paper sheet and the relation to the material's complex fibrous micro-structure.

Previous studies have shown that single paper fibers yield strong anisotropic swelling properties, i.e., on average, the fiber swells 20–30 more in transverse compared to longitudinal direction [2, 3, 4]. Inside the paper sheet, the significantly large transverse swelling is transmitted through the bonded regions to contribute to the sheet scale, as experimentally studied by Nanko and Wu [5]. It is appealing think that the moisture-induced dimensional change (hygro-expansion) of a paper sheet is dominated by the transverse fiber hygro-expansion. However, a theoretical composite framework [6] and 3D modelling of paper networks [7, 8] have shown that a large fraction of the sheet-scale hygro-expansivity is driven by the longitudinal fiber hygro-expansion. Additionally, these models showed that the longitudinal fiber hygro-expansion fully contributes to the sheet level and only a small portion of the transverse fiber hygro-expansion contributes, confirming the relevance of the longitudinal fiber hygro-expansion to the sheet-scale [6].

Paper sheet-scale measurements are usually performed on machine paper (oriented) and lab-made handsheets (random) [9, 10, 11], where the latter is more often considered when analyzing the difference between freely and restrained dried paper because the paper's properties can be tuned accordingly. Previous studies have shown that drying condition strongly affect the hygro-mechanical properties of the prepared paper sheet [5, 9, 12, 13, 14, 15, 16]. For instance, the

Young's modulus of restrained dried paper is significantly larger than freely dried paper because more fibers contribute to the load carrying after fiber straightening during drying [12, 13, 15]. Additionally, Jentzen [17] showed that single paper fibers dried under stress yield a higher stiffness and strength while they yield a lower micro-fibril angle. Regarding hygro-expansivity, restrained dried paper handsheets show a release of irreversible (dried-in) strain during the first wetting cycle and afterwards exhibit a larger hygro-expansivity, which is closer to the significantly larger hygro-expansivity of freely dried sheets [9, 14, 15, 15, 16]. The complex mechanisms behind the hygro-expansivity difference have been intensively studied in the past and various theories have been proposed.

Uesaka and Qi [18] proposed a micro-mechanical inter-fiber bond model to describe the hygro-expansivity difference, which was adopted in multiple works [14, 15, 16]. The model states, for restrained dried sheets, that the fibers forming the inter-fiber bonds are less wrapped around each other than for freely dried handsheets, due to the applied external stress during drying, resulting in a lower transverse strain transmission upon the bonded fiber and hence lower contribution to the sheet-scale hygro-expansivity. With recent advances in characterizations methods, Urstöger et al. [15] used X-ray computed tomography to characterize the inter-fiber bond geometries in freely and restrained dried handsheets and test the theory [18]. The authors identified three different inter-fiber bond geometries (in which (i) both fiber ends bent towards the bonded fiber, (ii) both ends away, and (iii) alternated; one towards and one away) and determined their frequency and wrap around angle. Interestingly, no significant difference was found between the two paper types, and hence it was concluded that difference in bond geometry cannot directly explain the hygro-expansion magnitude difference.

Van den Akker [19] argued that the hygro-expansion differences between machine (MD) and cross direction (CD) of machine paper were more attributed to differences made to the fiber structure during drying, than solely due to the fiber orientation distribution. Nanko and Wu [5], who studied the shrinkage of free and bonded segments inside freely and restrained dried handsheets, confirmed this by demonstrating the lower shrinkage of fibers aligned in MD (large tension), compared to fibers aligned in CD (little tension) inside the same handsheet, and attributed the difference to structural fiber changes. Additionally, Nanko and Wu [5] concluded that the significantly large transverse fiber shrinkage can compress the bonded fiber in longitudinal direction, similar to the findings of Page and Tydeman [20], and the freestanding parts are passively compressed or stretched by the surrounding fiber segments, all of which result in structurally different fibers inside the sheet after drying. Regarding the change in fiber structure, Salmén et al. [21] offered a comprehensive hypothesis to explain the hygro-expansivity difference between freely and restrained dried fibers, i.e., residual stress (dried-in strain) is stored inside the hemi-cellulose chains and cellulose micro-fibrils during

restrained drying, which, subsequently, restrict the fibers to swell upon wetting. In order to test if the difference in hygro-expansivity between freely and restrained dried handsheets is driven by the changes in fiber structure, hygro-expansion characterization of single fibers obtained from freely and restrained dried paper sheets is desired, which is the objective of this work.

To this end, we first propose a highly accurate single fiber swelling methodology which is significantly more accurate and enables transient hygro-expansion responses, compared to other than other single fiber (fibril) hygro-expansion methods proposed in the literature [4, 5, 22, 23, 24]. The method involves changing the relative humidity (RH) around a fiber, while consecutive topographies are obtained, which are afterwards correlated using a Global Digital Height Correlation (GDHC) algorithm to obtain the full-field (longitudinal, transverse, and shear) hygro-expansion [2, 3]. This method is subsequently employed to paper fibers subtracted from prepared freely and restrained dried paper handsheets. After performing sheet-scale hygro-expansion measurements, this approach enables a direct experimental comparison between the fiber and the sheet-scale characteristics, allowing identification of the longitudinal and transverse fiber hygro-expansion contributions.

In the following, first a handsheet hygro-expansion method is proposed, followed by a comprehensive explanation of the single fiber hygro-expansion method containing the rigorous derivation of the GDHC algorithm. In the results section, the hygro-expansivity of restrained and freely dried handsheet and single fiber picked from these handsheets are presented and discussed, and direct fiber-to-sheet comparison is performed. Finally, a conclusion is formulated.

MATERIALS AND METHODS

Preparation of the Handsheets

Freely and restrained dried handsheets with an average weight of ~60 g/m^2 were produced from bleached hardwood kraft pulp (Eucalyptus), using the "Rapid Kötchen" device, following the preparation method proposed by Larsson and Wågberg [14]. Please note that this pulp is the same as used for the single fiber hygro-expansion experiments conducted by Vonk et al. [3]. The freely dried handsheets were first pressed for 1 minute with a temperature of 93°C and pressure of 95 kPa and afterwards freely dried in a PTFE mesh drying frame to minimize out-of-plane deformation. Restrained dried handsheets were pressed for 10 minutes with a temperature of 93°C and pressure of 95 kPa. A 6 × 6 cm^2 sheet is obtained from each handsheet and a random pattern, for the Global Digital Image Correlation (GDIC) algorithm to track (discussed below), is applied using

charcoal sticks instead of using spray paint, of which the solvent could affect the fiber structure.

Handsheet Hygro-expansion Method

A non-contact full-field method based on GDIC is proposed to measure hygro-expansivity of the paper sheet. The method involves placing the prepared sheets between two woven steel gazes, which are spaced exactly the paper thickness from each other to minimize out-of-plane deformation. The structure is subsequently tested inside a climate box and captured using a camera system consisting of a telecentric lens. Telecentric lenses are specifically designed to have a centimeters long depth of focus, and hence do not measure any artificial strain due to (possible) out-of-plane deformations, which are known to occur during wetting of paper sheet [1]. The RH is accurately regulated by an external humidifier (*Cellkraft P-10 series*). One restrained and one freely dried handsheet is tested using six linearly increasing RH cycles from 30 – 90 – 30%, with a slope of 2%/min. Before testing, each sheet was climatized at 30% RH for 8 hours. The collected images (obtained once per minute) are correlated using a GDIC framework in which linear shape functions are used to find the displacement field while hygro-expansion (the main deformation mode) is of first order. Please note that the GDIC framework is similar the GDHC framework which is used for the single fiber hygro-expansivity tests which will be explained below. Finally, while the GDIC algorithms provides displacement fields, a linear strain definition is used to obtain the hygro-expansivity.

Preparation of the Single Fibers

The fibers are extracted from the (remainder of the) freely and constrained dried handsheets by mean of delaminating the paper sheet and cutting out the naturally sticking out fibers. A comprehensive analysis on 100 fibers picked from the handsheet showed that the morphology of the fibers was completely random in terms of straightness, twist, etc. Confirming that the fiber extraction procedure does not prefer specific fibers, and consequently, the fibers tested here are of random nature, representing the random structure of the paper sheet. Important to note is that even though the Eucalyptus fibers yield a micro-fibril angle of 0–13 degrees [25], which directly affects the fiber properties, the hardwood fibers obtained from the pulp bale showed little fiber-to-fiber variability [3]. Hence, the possible differences found here are mainly due to the drying history.

A schematic representation of the experimental methodology is shown in Figure 1 [2]. Two highly compliant (Ø50 μm) nylon wires are used to delicately fixate the fibers and maintain the fiber in the field of view (FOV) of the microscope.

The fiber is touched upon at two spots, providing full freedom for the hygro-expansion, while only minimizing rigid body motion, fiber twisting, and bending, displayed in Figure 1(a). The region of interest (ROI) of the fiber, which is captured by the microscope is always located in the center of the two wires. A polystyrene microparticle pattern is subsequently applied to the fiber using a dedicated mistification setup [26]. The specialty of this setup is that it can produce (micro- and nano-) particle patterns of particles sizes down to 50 nm, which is usually the biggest challenges in micro-mechanical DIC problems. In short, the setup generates a mist of particles and solvent (usually ethanol), which is subsequently heated up to evaporate the ethanol and obtain a flow of non-clustered particles which is blown onto the specimen where the particles maintain, resulting in a high-quality pattern without possibly affecting the specimen (fiber) surface. This micro-particle pattern is the most essential element required for the GDHC algorithm, while these particles are not affected by the hygroscopic changes and maintain on the fiber surface, as will be explained below.

Single Fiber Hygro-expansion Method

Regarding capturing the fiber surface structure, several options were considered. It was found that vertical scanning interferometry (VSI) (an optical microscopy method) is preferred over atomic force microscopy, which has been used before to measure the inter-fiber bond geometry, contact surface roughness and fiber surface roughness [27, 28, 29], since it is non-contact and has a small acquisition time with a relatively large FOV. Moreover, VSI was found to perform significantly better than confocal optical microscopy, while this is an intensity based profilometry technique and fiber tend to become more transparent during water absorption. Hence, in this work, VSI is used for the single fiber characterization. Since the fibers have diameters ranging from 20–30 μm, a 100× objective was chosen for the VSI profilometer (*Bruker NPFlex*), attaining a FOV of 60×80 μm^2 (1376×1040 pixels).

As shown in Figure 1(b), a prepared fiber is placed in a climate chamber underneath the optical profilometer. The same external humidifier as used for the sheet-scale experiments is used to regulate the RH inside the climate chamber. Before testing, the fiber is first equilibrated by maintaining the starting RH constant for 8 hours. During testing, the RH is gradually increased while the optical microscope takes consecutive topographies, during which the RH is captured. Finally, all experiments are performed at a temperature of 23°C.

The obtained fiber topographies are processed using a GDHC algorithm which was previously developed for a wide range of micro-mechanical problems to obtain full-field deformation data [30, 31, 32]. The GDHC algorithm has been

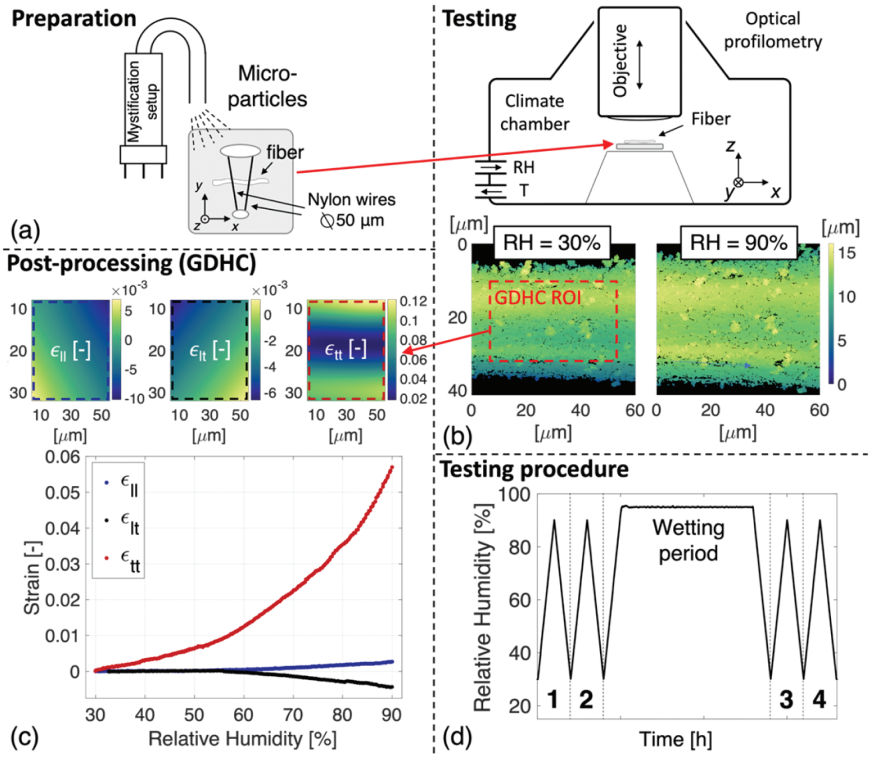

Figure 1. Schematic representation of the method with: (a) delicate clamping of the fiber by means of two nylon threads, onto which a micro-particle pattern is applied using a dedicated mistification setup [26], (b) the fiber is placed inside a climate chamber, in which the RH is controlled by an external humidifier, underneath an optical profilometer, allowing *in-situ* fiber hygro-expansion measurements, (c) the obtained topographies are correlated using a Global Digital Height Correlation to obtain the average longitudinal (ϵ_{ll}), transverse (ϵ_{tt}), and shear surface strain (ϵ_{lt}) of a single fiber, and (d) the specific RH course used to test the fibers.

adapted and optimized towards fiber hygro-expansion, as will be elaborated below. The GDHC algorithm enables determination of the three-dimensional displacement vector at each point of the ROI, allowing computation of the surface deformation and hence the fiber expansion. Combining these displacement field with the fiber topography enables determination of the longitudinal (ϵ_{ll}), and transverse (ϵ_{tt}) and shear surface strains (ϵ_{lt}), as shown in Figure 1(c). Subsequently determining the average strain value from the computed strain fields

enable the average ϵ_{ll}, ϵ_{tt}, and ϵ_{lt} as a function of RH. Please note that the full strain field is available to analyze possible inhomogeneous hygro-expansion.

Global Digital Height Correlation Algorithm Dedicated to Fiber Hygro-expansion

Digital Image Correlation (DIC) in its 2D form is a well-adopted image matching algorithm that allows full-field displacement measurements. It has been used for multiple paper mechanics problems, i.e., paper sheet-scale hygro-expansion measurements [16] and paper sheet under biaxial tension [33]. DIC exists in a "local" (subset) or a "global" (whole FOV) form [34, 35, 36], which have their own advantages and disadvantages. For fiber hygro-expansion measurements, Global DIC would be a better choice than DIC, since it is more robust against lost data and pattern degradation [37], which is known to occur when testing natural fibers. Additionally, it has been shown that GDIC can more easily be fine-tuned towards specific applications [38, 39, 40]. Here, however, while the 3D hygro-expansion of the fiber is desired, topographies are used instead of regular gray-scale images. Therefore, a Global Digital Height Correlation (GDHC) approach is adopted, which is based on topography conservation (instead of gray value conservation used for (G)DIC), i.e., the height value at pixel position $\vec{x}$ in the reference topography f is equal the height value at the new position $(\vec{x} + \vec{u}(\vec{x}))$ in the deformed topography g minus the out-of-plane displacement [41], which is:

$$\vec{\psi} = f(\vec{x}) - \left(g(\vec{x} + u(\vec{x})\vec{e}_x + v(\vec{x})\vec{e}_y) - w(\vec{x}) \right), \tag{1}$$

in which u and v are the in-plane displacement components in, respectively, x-direction ($\vec{e}_x$) and y-direction ($\vec{e}_y$), and w is the displacement in z-direction ($\vec{e}_z$), while ψ, the residual, represents acquisition noise and height distortions not captured by w. Note that both f and g contain height information as a function of the two-dimensional image coordinate system, hence the 3D displacement vector $(u(\vec{x}) = u(\vec{x})\vec{e}_x + v(\vec{x})\vec{e}_y + w(\vec{x})\vec{e}_z)$ is a function of the 2D position vector $(\vec{x} = x\vec{e}_x + y\vec{e}_y)$. ψ is minimized to find the optimal $u((\vec{x}))$, i.e.:

$$\text{argmin}_{\underline{u}(\vec{x})}(\Psi) = \text{argmin}_{\underline{u}(\vec{x})}\left(\int_\Omega \psi^2 d\vec{x}\right), \tag{2}$$

in which Ω is the global ROI, as shown in Figure 1(b). While finding thee unknown values per known pixel states an ill-posed problem, the number of degrees of freedom (DOF) need to be reduced. Hence, to this end, an approximated displacement field, $\vec{u}^*(\vec{x}, \underline{\lambda})$, is introduced, spanned by shape functions, $\vec{\phi}(\vec{x})$, associated with reduced DOF, $\underline{\lambda}$;

$$\left\{ \bar{\gamma}_x, \bar{\gamma}_y, \bar{\gamma}_z \right\} = \bar{\gamma} \text{ with } w_* \underset{\leftarrow}{n} = (\bar{\gamma}, \underset{\leftarrow}{x})_* \underset{\leftarrow}{n} = (\bar{\gamma}, \underset{\leftarrow}{x})_* \underset{\leftarrow}{n} \partial_x \underset{\leftarrow}{(x)} + (\bar{\gamma}, \underset{\leftarrow}{x})_* \underset{\leftarrow}{n} \partial_y \underset{\leftarrow}{(x)} + (\bar{\gamma}, \underset{\leftarrow}{x})_* \underset{\leftarrow}{n} \partial_z \underset{\leftarrow}{(x)} \text{ with } \underset{\leftarrow}{n} = \sum_{t=1}^{n} \gamma_x^t \phi_x^t \partial_x \underset{\leftarrow}{(x)} + \sum_{f=1}^{n} \gamma_y^f \phi_y^f \partial_y \underset{\leftarrow}{(x)} + \sum_{k=1}^{n} \gamma_z^k \phi_z^k \partial_z \underset{\leftarrow}{(x)} \cdot \quad (3)$$

The goal is to minimize Ψ using the $3n$ shape functions with DOF $\underline{\lambda}$, where ϕ_i is a series of basis functions that should be rich enough to capture the fiber swelling kinematics and $\underline{\lambda}$ are to be determined. Equation 2 then transforms into:

$$\text{argmin}_{\underline{\lambda}} \Psi(\underline{\lambda}). \quad (4)$$

The solution of this non-linear minimization problem is found by employing an iterative modified Newton-Raphson scheme, which has been derived in a consistent manner [35]. More details of the derivation of the above given GDHC algorithm can be found in [2, 35, 41].

GDHC allows shape functions of all sorts to be implemented in the algorithm, however, polynomials or B-spline grids are mostly adopted. The optimal basis function and order required to capture the minimal kinematically admissible 3D displacement field which completely describes the fiber swelling kinematics can be determined before testing. This optimal kinematic regularization must contain the following three displacement, three rotation and six deformation (expansion and bending) modes [2]:

- rigid body translation in the three principal directions (0^{th}-order polynomial),
- homogeneous hygroscopic expansion along three principal directions (1^{st}-order polynomial),
- rotation around the three principal directions (1^{st}-order polynomial),
- bending in all three directions (2^{nd}-order polynomial).

In the case of fiber hygro-expansion, a 2^{nd} order polynomial is sufficiently rich to capture the fiber hygro-expansion kinematics and is used for the single fibers. Validation of this optimal kinematic regularization is performed in [2], where the order of the polynomial is changed and the residual value (which should be lower for a more optimal regularization) is analyzed, similar to the analysis done by Neggers et al. [41] and Hoefnagels et al. [42].

The gradient of the topography in the end drives the GDHC algorithm, which implies that the micro-particle pattern must reveal sufficient gradients to properly find convergence and determine the displacement field. This is of course also the reason why a micro-particle pattern is applied to the fiber. Unfortunately, the edges of the particles are difficult to measure using VSI, while steep angle at the edges of the particles result in data loss, also interference patterns are sometimes

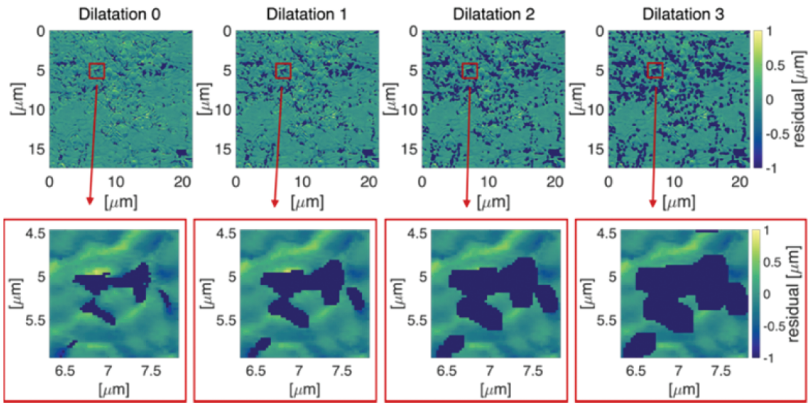

Figure 2. The dilatation algorithms which is used to mask high residual regions that can make the correlation unstable. A paper fiber is subjected to an RH cycle from 50 to 80%, of which the residual field between the first and last topography is shown, with zoomed view to highlight the regions of lost data around a 500 nm particle. A dilatation of 0 (initial topography) – 3 rows around a NaN pixel are depicted. A dilatation of 2 was found to perform the best, while it masks out the higher residual regions while still maintaining the particle geometry and is hence chosen for all fiber correlations [2].

visible. These regions in turn result in higher residual values. Therefore, a masking algorithm is proposed to minimize this phenomenon, which is explained by a paper fiber which is subjected to a RH change from 50 to 80%, of which the residual field between the first and the last topography is given in Figure 2. A zoomed view is provided in which a 500 nm particle, with a region of lost datapoints around them, is visible. These lost regions (not a number (NaN)) originate from the sharp edges of the particle, which could not be captured by the microscope. Consequently, higher residual values are found around the regions of missing data, which could make the correlation unstable. Therefore, a dilatation algorithm is applied to mask out pixels around the NaN pixels in the reference topography which turn up as higher residual values. A dilatation of 0 results to the initial topography, while a dilatation of *n*, mask a band of n pixels around a NaN pixel in the reference topography, shown in Figure 2. Masking out these pixels has the advantage that higher residual values are covered, but the disadvantage is that the quality of the image gradient (the pattern) is reduced, as can be seen for a dilatation of 3, where the 500 nm particle is almost completely masked out. In the following, a dilatation of 2 is used for all correlations, which resembles a good balance [2].

Precision and Applicability

Initial precision studies of the above-described method showed a longitudinal and transverse surface strain precision of $1{\cdot}10^{-4}$ and $7{\cdot}10^{-4}$ for paper fibers [2]. However, in that work, a regular airbrush with a solution of microparticles and ethanol was used to apply the pattern, which resulted in non-ideal (clustered) patterns. Hence in a follow up paper [3] and in this work, the mistification setup was employed, resulting in significantly improved pattern quality, which in turn resulted in a better longitudinal and transverse surface strain precision of $1{\cdot}10^{-4}$ and $2{\cdot}10^{-4}$. Furthermore, as elaborated in [2], the method is also applicable to different fiber types, e.g., viscose and 3D-printed hydrogels [43]. Finally, to highlight the versatility and tunability of the proposed fiber hygro-expansion GDHC algorithm, adaptations have been made in order to track large deformations during rapid swelling of different types of supramolecular hydrogels [44], by means of transforming the framework into an incremental (each topography is correlated to its previous topography) instead of classical GDHC framework (where each topography is correlated back to the first topography), to become less sensitive to unavoidable surface instabilities which are known to occur during hydrogel swelling [45], which make the correlation unstable.

Testing Strategy

Each fiber is prepared accordingly and subjected to two cycles from 30 – 90 – 30% RH (cycle 1 & 2) as shown in Figure 1(d). Then, a long duration cycle from 30 – 95 – 30% RH is entered, where the 95% RH set point is kept constant for 8 or 24 hours for the fibers picked from, respectively, the freely and restrained dried handsheets. This period is referred to as the wetting period. Afterwards, the fiber is again subjected to two cycles from 30 – 90 – 30%, RH (cycle 3 & 4). Each change in RH setpoint was performed with a RH rate of 1%/min. This specific RH strategy is chosen to analyze if an initially "restrained dried fiber" can transform into a "freely dried fiber" after being subjected to a longer wetting period in which the initial dried-in strain is released.

RESULTS AND DISCUSSION

Handsheet Hygro-expansivity

The sheet-scale hygro-expansion response of the restrained and freely dried handsheet is given in Figure 3. The hygro-expansivity of the freely dried handsheets is significantly larger than the restrained dried handsheet, similar to works earlier reported in literature [5, 9, 14, 15]. Furthermore, the restrained dried handsheet

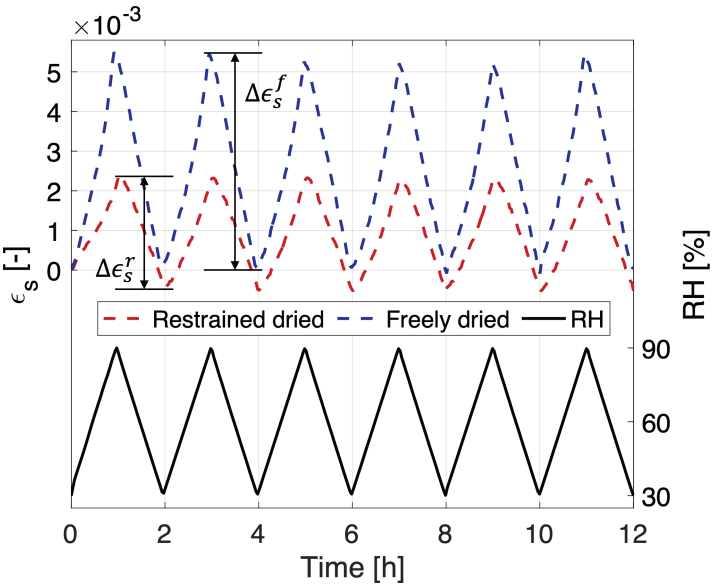

Figure 3. Hygro-expansion response of a freely and restrained dried handsheet. The hygro-expansivity of the freely dried handsheets is significantly larger, similar to earlier works [5, 9, 14, 15].

shows only a slight release of dried-in strain, compared to other works [9, 14], which is attributed to the handsheets being produced by *Mondi Group* (Vienna, Austria) before being tested. The environmental conditions during shipment are of course unknown, and the release of dried-in strain could already have happened. However, the significant hygro-expansivity difference is still visible (which is the main objective of this work), and hence the handsheets are suitable for this study. Next, the handsheets show cyclic repeatability, highlighting the reproducibility of the proposed method. Finally, the average shrinkage per drying slope for the freely ($\Delta\epsilon_s^f$) and restrained dried handsheets ($\Delta\epsilon_s^r$) are extracted and it was found that the freely and restrained dried handsheets shrink, on average, 0.00532 ± 0.00008 and 0.00281 ± 0.00002, respectively for an RH change from 90 to 30%, considering the six cycles.

Single Fiber Hygro-expansivity

The preliminary hygro-expansion response of a freely dried fiber is given in Figure 4(a). First, the strong anisotropic swelling behavior which the fiber exhibit,

as was studied in [2, 3], is visible. Furthermore, as expected, a plateau value is found for ϵ_{tt} the during the wetting period (and for ϵ_{ll} and ϵ_{lt} at the end of the wetting period), implying saturation of the moisture content and only slight release of possible dried-in strain. The hygro-expansion during the drying slope of cycles 1 & 2 and 3 & 4 are very similar, with a slight exception of ϵ_{lt}. A similar response was found for four more fibers picked from the freely dried handsheet.

The preliminary hygro-expansion response of a fiber picked from a restrained dried handsheet is given in Figure 4(b). First, the ϵ_{ll} and ϵ_{lt} hygro-expansivity before the wetting period is significantly lower compared to the fibers picked from the freely dried handsheet, confirming that the fibers are structurally different as previously demonstrated [5, 19, 20]. Furthermore, a clear release of dried-in strain occurs during the wetting period; (i) ϵ_{tt} shows an ongoing increasing trend, possibly due to the release of dried-in strain, and (ii) ϵ_{ll} and ϵ_{lt}, respectively, show a significantly larger decrease or increase during the drying slope after the wetting period. This release of the stored dried-in strain most likely drives the larger hygro-expansivity after the wetting period [21], which is (mainly for ϵ_{ll} and ϵ_{lt}) comparable to the hygro-expansivity of the fibers picked from the freely dried handsheet shown in Figure 4(a).

Unfortunately, not all restrained dried fiber showed the district release of dried-in strain as given in Figure 4(b), implying that the moisture content, for some cases, was not sufficient to completely release the dried-in strain stored in the fiber [21]. Hence, for a future publication [46], a setup is developed which enables cooling the fiber to reach higher moisture content levels. Preliminary results seem to show that the hygro-expansion responses are much cleaner with this new setup in terms of more reproducible behavior during the wetting period.

Comparing the freely and restrained dried hygro-expansion responses, the ϵ_{ll} and ϵ_{lt} before the wetting period is significantly lower for the restrained dried fiber. Furthermore, when it comes to release of dried-in strain, it seems that both fibers show a release in ϵ_{ll} of approximately 0.002 between the start and end of the RH trajectory. A reasonable explanation for this is that the fibers in both sheets were affected by neighboring fiber segments, leading to a spread in dried-in strain per fiber, as studied by Nanko and Wu [5]. To put this into numbers, the average shrinkage in ϵ_{ll} considering all free and restrained fibers is, respectively, 0.0006 ± 0.0019 and 0.0021 ± 0.0028, indicating that the freely dried fiber response shown in Figure 4(a) displays a larger release of negative dried-in strain compared to the other freely dried fibers. Some freely dried fibers showed a release of positive dried-in strain which can of course be attributed to the micro-compressions stored inside the fiber in the bonded regions during paper drying [5, 20], while only one restrained dried fiber showed a positive release of dried-in strain.

To conduct a direct comparison between the restrained and freely dried fibers, the decrease in longitudinal ($\Delta\epsilon_{ll}$), transverse ($\Delta\epsilon_{tt}$), and shear hygro-expansion ($\Delta\epsilon_{lt}$) for cycle 1–4 are extracted, as annotated in Figure 4(a).

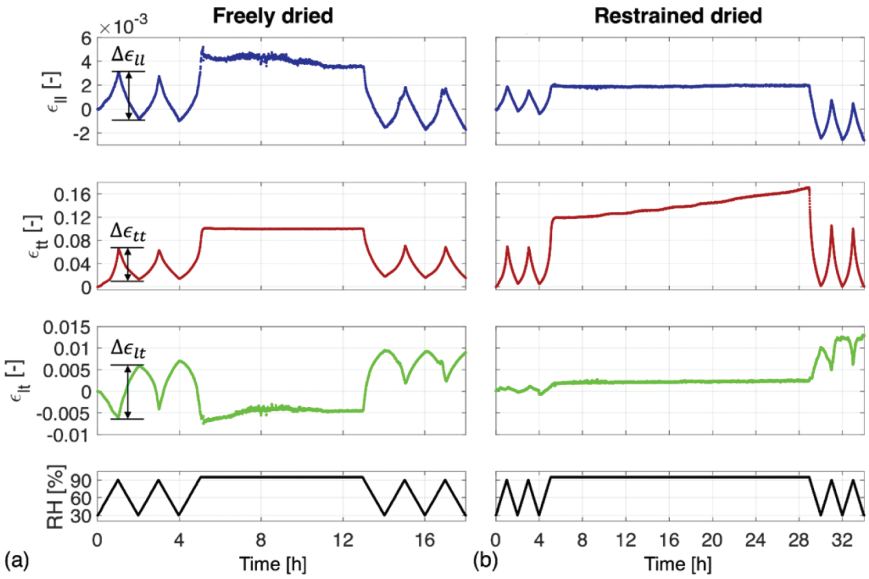

Figure 4. Preliminary results of the hygroscopic response of fibers picked from (a) a freely dried and (b) a restrained dried handsheet. The fiber picked from the freely dried handsheets shows no clear release of dried-in strain and the hygro-expansion response of cycle 1 & 2 are similar to cycle 3 & 4 and the hygro-expansivity is similar before and after the wetting period. The fiber picked from the restrained dried handsheet, however, shows a significant release of dried-in strain visualized by the ongoing increasing ϵ_{lt} and the dip in ϵ_{ll}, respectively, during and after the wetting period. Consequently, the hygro-expansivity before and after the wetting period are distinctly different. The hygro-expansion decrease for every cycle ($\Delta\epsilon_{ll}$, $\Delta\epsilon_{tt}$, and $\Delta\epsilon_{lt}$), as annotated in (a), are subtracted. Improved results for the fully saturated specimen during the wetting period (instead of the here presented 95% RH) will be published in a future publication [46].

Freely and Restrained Dried Fiber Comparison

The average and standard deviation of the hygro-expansion decrease of cycles 1–4 for five freely and twelve restrained dried fibers are given in Figure 5. When looking at the freely dried fibers, very reproducible behavior is found considering all fibers and the standard deviations are low, hence implying low cycle-to-cycle and fiber-to-fiber variability, also highlighting the reproducibility of the proposed fiber hygro-expansion methodology. Only $\Delta\epsilon_{lt}$ deviates while the spread after the wetting period significantly decreased. Finally, it seems that the hygro-expansivity before and after the wetting period is comparable, similar to Figure 4(a).

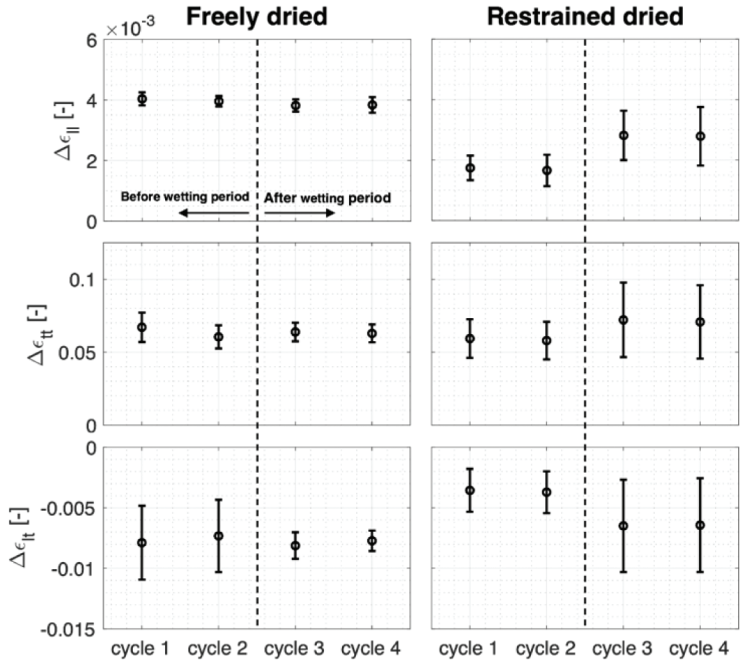

Figure 5. Preliminary results of the average longitudinal, ($\Delta\epsilon_{ll}$), transverse ($\Delta\epsilon_{tt}$) and shear hygro-expansion decrease ($\Delta\epsilon_{lt}$) of five fibers picked from a freely and twelve fibers from a constrained dried handsheet. Improved results for the fully saturated specimen during the wetting period (instead of the here presented 95% RH) will be published in a future publication [46].

For the restrained dried fibers, a larger hygro-expansivity is found after the wetting period, suggesting that the release of dried-in strain enables the larger hygro-expansivity. Furthermore, a significantly large spread in $\Delta\epsilon_{ll}$, $\Delta\epsilon_{tt}$, and $\Delta\epsilon_{lt}$ is found after the wetting period, which is attributed to the fact that not all fiber showed distinctly different behavior before and after the wetting period, implying that some fibers did not fully release the stored dried-in strain to transform into a "freely dried fiber". As already mentioned, this is remedied in a future paper [46] in which a setup is proposed that enables higher moisture content levels.

When considering the average $\Delta\epsilon_{ll}$, $\Delta\epsilon_{tt}$, and $\Delta\epsilon_{lt}$ and standard deviation before the wetting period of all freely and restrained dried fibers, it can be concluded that, on average, the hygro-expansivity of the freely dried fibers is 2.35±0.81 larger in longitudinal, 1.09±0.42 larger in transverse, 2.09±1.89 larger in shear direction

compared to restrained dried fibers. Looking at these numbers, it seems that restrained drying mainly affects the fiber's longitudinal and shear hygro-expansivity, similar to the findings of Nanko and Wu [4]. The physical origin of the phenomena occurring in the complex fiber wall structure which drive these hygro-expansivity differences will be comprehensively explained in a future publication [46].

Finally, it seems that the sheet-scale hygro-expansivity ($\Delta\epsilon_s^r$ and $\Delta\epsilon_s^f$) is slightly higher than the longitudinal fiber hygro-expansion for both handsheets, confirming the relevance of the longitudinal hygro-expansivity to the sheet scale as generally adopted [6, 8]. The remainder should be provided by the transverse fiber hygro-expansivity which is transmitted though the bonded regions. For both handsheets types, this contribution is relatively low, as was also found by [7] and experimentally shown in a future publication in which the full-field hygro-expansivity of four isolated inter-fiber bonds is investigated [47].

CONCLUSION

In this work, we studied the hygro-expansivity of freely and restrained dried handsheets and single fibers picked from freely and restrained dried handsheets. To do so, a dedicated single fiber hygro-expansivity method was proposed which is based on Global Digital Height Correlation (GDHC). The method enabled the transient full-field hygro-expansion during wetting and drying. It involved (i) delicately clamping the fiber to allow full hygroscopic freedom while minimizing rigid body motion, rotation and bending, (ii) testing the fiber inside a climate chamber, in which the relative humidity (RH) is varied, underneath an optical profilometer, and (iii) correlating the obtained topographies using a GDHC algorithm to obtain the longitudinal, transverse and shear hygro-expansion.

Each fiber was subjected to two 30 – 90 – 30% RH cycles followed by a longer period of 95% RH (wetting period), after which the same two RH cycles are employed. The results revealed insightful novel data, i.e., it was found that (i) the hygro-expansivity of fibers picked from the freely dried handsheet was comparable before and after the wetting period, in contrast to (ii) the restrained dried fibers, which showed a distinctly larger hygro-expansivity after the wetting period, (iii) the fibers picked from the restrained dried handsheet revealed a 2.35±0.81 lower longitudinal, 1.09±0.42 lower transverse, 2.09±1.89 lower shear hygro-expansivity as the fiber picked from the freely dried handsheet, and (iv) the transverse fiber hygro-expansion contribution to the sheet scale is relatively low, confirming the generally accepted relevance of the longitudinal fiber hygro-expansion to the sheet-scale. While these experiments are key for re-understanding

the hygro-expansion magnitude difference, more research need to be done on the driving mechanism inside the fiber wall structure, the influence of wood type, and how the single fiber characteristics translate towards the sheet-scale via, i.e. numerical modeling.

REFERENCES

[1] Kulachenko, A., Gradin, P. and Uesaka, T. (2005). Tension Wrinkling and Fluting in Heatset Web Offset Printing process. Post buckling analyses. In *13th Fundamental Research Symposium on Advances in Paper Science and Technology*, Cambridge, England, Sepember 2005 (pp. 1075–1099). The Pulp and Paper Fundamental Research Society.

[2] Vonk, N. H., Verschuur, N. A. M., Peerlings, R. H. J., Geers, M. G. D. and Hoefnagels, J. P. M. (2020). Robust and precise identification of the hygro-expansion of single fibers: a full-field fiber topography correlation approach. *Cellulose*, 27: 6777–6792.

[3] Vonk, N. H., Geers, M. G. D. and Hoefnagels, J. P. M. (2021). Full-field hygro-expansion characterization of single softwood and hardwood pulp fibers. *Nordic Pulp & Paper Research Journal*, 36(1): 61–74.

[4] Joffre, T., Isaksson, P., Dumont, P. J., Du Roscoat, S. R., Sticko, S., Orgéas, L. and Gamstedt, E. K. (2016). A method to measure moisture induced swelling properties of a single wood cell. *Experimental Mechanics*, 56(5): 723–733.

[5] Nanko, H. and Wu, J. (1995). Mechanisms of paper shrinkage during drying. In *International Paper Physics Conference*, Niagara-on-the-Lake, Canada (pp. 103–113).

[6] Uesaka, T. (1994) General formula for hygroexpansion of paper. *Journal of Material Science*, 29(9): 2373–2377

[7] Brandberg, A., Motamedian, H. R., Kulachenko, A. and Hirn, U. (2020). The role of the fiber and the bond in the hygroexpansion and curl of thin freely dried paper sheets. *International Journal of Solids and Structures*, 193: 302–313.

[8] Motamedian, H. R. and Kulachenko, A. (2019). Simulating the hygroexpansion of paper using a 3d beam network model and concurrent multiscale approach. International *Journal of Solids and Structures*, 161: 23–41.

[9] Uesaka, T., Moss, C. and Nanri, Y. (1992). The characterization of hygroexpansivity of paper. *Journal of Pulp and Paper Science*, 18(1): J11–J16.

[10] Lavrykov, S. A., Ramarao, B. V. and Lyne, O. L. (2004). The planar transient hygroexpansion of copy paper: experiments and analysis. *Nordic Pulp & Paper Research Journal*, 19(2): 183–190.

[11] Niskanen, K. J., Kuskowski, S. J. and Bronkhorst, C. A. (1997). Dynamic hygroexpansion of paperboards. *Nordic Pulp & Paper Research Journal*, 12(2): 103–110.

[12] Kouko, J., Retulainen, E. and Kekko, P. (2014). Influence of straining during wet pressing and drying on strength properties of paper. *Nordic Pulp & Paper Research Journal*, 29(3): 453–461

[13] Mäkelä, P. (2009, September). Effect of drying conditions on the tensile properties of paper. In *Transactions of the 14th Fundamental Research Symposium*, Oxford (pp. 1079–1094).
[14] Larsson, P. A. and Wågberg, L. (2008). Influence of fibre–fibre joint properties on the dimensional stability of paper. *Cellulose*, 15(4): 515–525.
[15] Urstöger, G., Kulachenko, A., Schennach, R. and Hirn, U. (2020). Microstructure and mechanical properties of free and restrained dried paper: a comprehensive investigation. *Cellulose*, 27(15): 8567–8583.
[16] Fellers, C. (2009) The interaction of paper with water vapour. In: *Pulping Chemistry and Technology*, Eds. Ek, M., Gellerstedt, G., Henriksson, G., Vol. 2. Walter de Gruyter, Berlin.
[17] Jentzen, C. A. (1964). "The effect of stress applied during drying on some of the properties of individual pulp fibers" (Doctoral dissertation, Georgia Institute of Technology).
[18] Uesaka, T. and Qi, D. (1994) Hygroexpansivity of paper: effects of fibre-to-fibre bonding. *Journal of Pulp and Paper Science* 20(6): J175–J179
[19] Van den Akker, J. A. (1961). Some theoretical considerations on the mechanical properties of fibrous structures. In *Symposium Transactions*. Technical section of the British Paper and Board Maker's Association.
[20] Page D. H, Tydeman P (1962) A new theory of the shrinkage, structure and properties of paper. In: Bolam F (ed) *The Formation and Structure of Paper*, Technical Section British Paper and Boards Makers' Association, London, vol 1., pp. 397–425
[21] Salmén, L., Fellers, C. and Htun, M. (1987). The development and release of dried-in stresses in paper. *Nordic Pulp & Paper Research Journal*, 2(2): 44–48.
[22] Meylan, B.A. (1972) The influence of micro-fibril angle on the longitudinal shrinkage–moisture content relationship. *Wood Science and Technology*, 6: 293–301
[23] Lee, J. M., Pawlak, J. J. and Heitmann, J. A. (2010) Longitudinal and concurrent dimensional changes of cellulose aggregate fibrils during sorption stages. *Materials Characterization*, 61: 507–517
[24] Tydeman, P. A., Wembridge, D. R. and Page, D. H. (1965) Transverse shrinkage of individual fibres by micro-radiography. In: *Consolidation of the Paper Web*. Transcript of the IIIrd Fundamental Research Symposium, Cambridge, pp. 119–144.
[25] French, J., Conn, A. B., Batchelor, W. J. and Parker, I. H. (2000). The effect of fibre fibril angle on some handsheet mechanical properties. *Appita journal*, 210–215.
[26] Shafqat, S. and Hoefnagels, J. P. M. (2021). Cool, Dry, Nano-scale DIC Patterning of Delicate, Heterogeneous, Non-planar Specimens by Micro-mist Nebulization. *Experimental Mechanics*, 1–21.
[27] Schmied, F. J., Teichert, C., Kappel, L., Hirn, U., Bauer, W. and Schennach, R. (2013). What holds paper together: Nanometre scale exploration of bonding between paper fibres. *Scientific Reports*, 3(1): 1–6.
[28] Hirn, U. and Schennach, R. (2015). Comprehensive analysis of individual pulp fiber bonds quantifies the mechanisms of fiber bonding in paper. *Scientific Reports*, 5(1): 1–9.
[29] Ganser, C., Hirn, U., Rohm, S., Schennach, R. and Teichert, C. (2014). AFM nanoindentation of pulp fibers and thin cellulose films at varying relative humidity. *Holzforschung*, 68(1): 53–60.

[30] Han, K., Ciccotti, M. and Roux, S. (2010). Measuring nanoscale stress intensity factors with an atomic force microscope. *EPL* (*Europhysics Letters*), 89(6): 66003.
[31] Van Beeck, J., Neggers, J., Schreurs, P. J. G., Hoefnagels, J. P. M. and Geers, M. G. D. (2013) Quantification of three-dimensional surface deformation using global digital image correlation. *Experimental Mechanics*. 54: 557–570
[32] Shafqat, S., Van der Sluis, O., Geers, M. and Hoefnagels, J. (2018). A bulge test based methodology for characterizing ultra-thin buckled membranes. *Thin Solid Films*, 660: 88–100.
[33] Alzweighi, M., Mansour, R., Tryding, J. and Kulachenko, A. (2022). Evaluation of Hoffman and Xia plasticity models against bi-axial tension experiments of planar fiber network materials. *International Journal of Solids and Structures*, 238: 111358.
[34] Bruck, H. A., McNeill, S. R., Sutton, M. A. and Peters, W. H. (1989) Digital image correlation using Newton–Raphson method of partial differential correction. *Experimental Mechanics*. 29: 261–267
[35] Neggers, J., Blaysat, B., Hoefnagels, J. P. M. and Geers, M. G. D. (2016) On image gradients in digital image correlation. *International Journal for Numerical Methods in Engineering* 105(4): 243–260
[36] Hild, F. and Roux, S. (2012) Comparison of local and global approaches to digital image correlation. *Experimental Mechanics*, 52: 1503–1519
[37] Bergers, L. I. J. C., Neggers, J., Geers, M. G. D. and Hoefnagels, J. P. M. (2013) Enhanced global digital image correlation for accurate measurement of microbeam bending. *Advanced Materials Modelling for Structures*, 19: 42–52
[38] Neggers, J., Hoefnagels, J. P. M., Hild, F., Roux, S. and Geers, M. G. D. (2012) Global digital image correlation enhanced full-field bulge test method. *Proceedings IUTAM*, 4: 73–81
[39] Kleinendorst, S. M., Hoefnagels, J. P. M., Fleerakkers, R. C., van Maris, M. P. F. H. L., Cattarinuzzi, E., Verhoosel, C.V. and Geers, M.G.D. (2016) Adaptive isogeometric digital height correlation: application to stretchable electronics. *Strain*, 52: 336–354
[40] Kleinendorst, S. M., Hoefnagels, J. P. M. and Geers, M. G. D. (2019). Mechanical Shape Correlation: A novel integrated digital image correlation approach. *Computer Methods in Applied Mechanics and Engineering*, 345: 983–1006.
[41] Neggers, J., Hoefnagels, J. P. M., Hild, F., Roux, S. and Geers, M. G. D. (2014). Direct stress-strain measurements from bulged membranes using topography image correlation. *Experimental Mechanics*, 54(5): 717–727.
[42] Hoefnagels, J. P. M., van Dam, K., Vonk, N. and Jacobs, L. (2021). Accurate Strain Field Measurement During Strip Rolling by Exploiting Recurring Material Motion with Time-Integrated Digital Image Correlation. *Experimental Mechanics*, 1–23.
[43] Wu, D. J., Vonk, N. H., Lamers, B. A., Castilho, M., Malda, J., Hoefnagels, J. P. and Dankers, P. Y. (2020). Anisotropic hygro-expansion in hydrogel fibers owing to uniting 3D electrowriting and supramolecular polymer assembly. *European Polymer Journal*, 141: 110099.
[44] Vonk, N. H., Adrichem, S. C. A., Wu, D. J., Dankers, P. Y. W. and Hoefnagels, J. P. M. Full-field hygroscopic characterization of 3D-printed supramolecular hydrogels (in preparation)

[45] Bertrand, T., Peixinho, J., Mukhopadhyay, S. and MacMinn, C. W. (2016). Dynamics of swelling and drying in a spherical gel. *Physical Review Applied*, 6(6): 064010.
[46] Vonk, N. H., Peerlings, R. H. J., Geers, M. G. D. and Hoefnagels, J. P. M. Revisiting the hygro-expansion of restrained and freely dried paper sheets – from fiber to network coupling (in preparation)
[47] Vonk, N. H., Peerlings, R. H. J., Geers, M. G. D. and Hoefnagels, J. P. M. Full-field, quasi-3D hygro-mechanics of isolated paper inter-fiber bonds (in preparation)